Electromagnetic wave propagation through realistic inhomogeneous turbulence

Victor Darchy, Rémi Douvenot, Stéphane Jamme, Hélène Galiègue

Electromagnetic Wave Propagation Through Realistic Inhomogeneous Turbulence

Victor Darchy, Rémi Douvenot, Stéphane Jamme, and Hélène Galiègue

Abstract – The marine atmospheric boundary layer (MABL) is an intricate environment where diverse atmospheric phenomena can affect electromagnetic (EM) systems. The stochastic multiple phase screen method (sMPS) is conventionally used to model the impact of tropospheric turbulence on EM wave propagation. It often relies on the use of homogeneous Kolmogorov spectra. This study presents two original methods for generating inhomogeneous turbulence with sMPS. The LES-Kolmogorov approach uses accurate turbulent structure constant profiles directly extracted from atmospheric simulations, while the Bump-Kolmogorov method (BK model) approximately replicates it with a parametric model. Log-amplitude profile computations highlight the specific impact of turbulence inhomogeneity. The proposed methods show good agreement, suggesting the feasibility of an accurate parametric replication of turbulence in the MABL.

1. Introduction

The marine atmospheric boundary layer (MABL) is a complex environment where various atmospheric phenomena can affect electromagnetic (EM) systems. In particular, tropospheric turbulence results in fine-scale fluctuations of the atmospheric refractive index that can introduce perturbations in both the amplitude and phase of EM signals, thereby inducing additional losses. Thus, comprehensive turbulence modeling is essential to quantitatively assess the influence of the atmosphere on the propagation of EM waves.

Split-step methods are widely employed for modeling long-range propagation within complex media by solving the 2D parabolic wave equation [1–3]. A vertical phase screen is applied to the propagated signal to account for the contribution of the atmosphere. In the case of atmospheric turbulence, the stochastic multiple-phase screen method (sMPS) is classically used [3–5]. This is based on the Tatarskii theory [6], which considers turbulent phase screens as stochastic processes generated from homogeneous Kolmogorov spectra. However, the MABL heat and moisture exchanges between the atmosphere and the ocean surface result in vertical inhomogeneities of turbulence that can impact the propagation of EM waves [7, 8].

The large eddy simulation (LES) is a numerical method for solving the Navier-Stokes equations, aiming at capturing large-scale turbulent structures. It can be used to generate ABLs and study their characteristics [9, 10] and, therefore, to better understand the impact of atmospheric turbulence on EM wave propagation [11–13].

The objective of this letter was to compute realistic turbulent phase screens representative of a MABL using sMPS. An inhomogeneous formulation of the classical Von-Karman Kolmogorov spectrum was initially computed from the results of the LES of a tropical MABL. Subsequently, a reproduction of this inhomogeneity was proposed using a parametric model. The free-space propagations resulting from these two approaches were ultimately compared with the case of an equivalent homogeneous turbulence.

This paper is organized as follows: Section 2 focuses on the development of the two methods for generating inhomogeneous turbulent atmospheres. Section 3 compares these approaches through numerical simulations.

2. Generation of a Realistic Inhomogeneous Turbulence

This section introduces a realistic vertical inhomogeneity in the random realizations of turbulent phase generated from a Von-Karman Kolmogorov spectrum. First, the formalism of the sMPS method is reminded. The vertical profiles of the outer scale length and turbulent structure constant are then directly extracted from the output of the LES of a tropical MABL to compute a realistic "LES-Kolmogorov" spectrum. The obtained inhomogeneous behavior is finally analytically replicated using a parametric model.

In the following, the EM propagation is studied in a 2D configuration. The horizontal x-axis denotes the direction of propagation, while z indicates the vertical.

2.1 Overview of the Stochastic Multiple Phase Screen Method

Tropospheric turbulence is characterized by chaotic variations of the thermodynamic fields that induce fast refractive index fluctuations. Hence, n is traditionally represented by a deterministic average value $\langle n \rangle$ and a random fluctuating component Δn so that $n = \langle n \rangle + \Delta n$. The mean refractive index profile is here considered homogeneous so that $\langle n \rangle = 1$, which leads to the definition of a 1D vertical turbulent phase screen,

Manuscript received 10 November 2023.

Victor Darchy, Rémi Douvenot, and Hélène Galiègue are with ENAC, ISAE-SUPAERO, Université de Toulouse, 7 Avenue Édouard Belin, Toulouse, France; e-mail: victor.darchy-ext@enac.fr, remi.douvenot@enac.fr, helene.galiegue@enac.fr.

Stéphane Jamme is with ISAE-SUPAERO, Université de Toulouse, 10 Avenue Édouard Belin, Toulouse, France; e-mail: stephane.jamme@isae-supaero.fr.

$$\Phi_{x+\Delta_x}(z) = k_0 \int_x^{x+\Delta_x} \Delta n(x', z) \mathrm{d}x'. \quad (1)$$

k_0 corresponds to the EM wave number in the vacuum, and Δ_x is the propagation step. The conventional sMPS method [3–6] consists in generating random realizations of Φ by filtering a Gaussian white noise with a Von-Karman Kolmogorov spectrum [14] defined as

$$S_\Phi(k_z) = 2\pi k_0^2 \Delta_x 0.055 C_n^2 \left(k_z^2 + \left(\frac{2\pi}{L_{\mathrm{os}}} \right)^2 \right)^{-4/3}. \quad (2)$$

This formulation provides a reasonable spectral profile for the energetic length scales of turbulence (i.e., for $k_z < 2\pi/L_{\mathrm{os}}$) and follows the Kolmogorov theory in the inertial subrange of scales (i.e., $2\pi/L_{\mathrm{os}} < k_z < 2\pi/L_{\mathrm{is}}$). L_{os} and L_{is} are the outer and inner scale lengths of turbulence, respectively. C_n^2 indicates the turbulent structure constant that quantifies the turbulence intensity, and k_z corresponds to the vertical component of the spectral variable. The major limitation of this method lies in the vertical homogeneity of the modeled turbulence intensity, which does not accurately represent the real behavior of an ABL [7, 8, 11]. Thus, the main objective of this paper was to introduce a realistic vertical dependency in the turbulent structure constant $C_n^2(z)$.

2.2 Inhomogeneous Turbulence From Atmospheric Simulations

The tropospheric RF refractive index is linked to the thermodynamic fields by [15]

$$n = 1 + n_{\mathrm{d}} + n_{\mathrm{w}}, \quad (3)$$

with

$$\begin{cases} n_{\mathrm{d}} = (77.60 \dfrac{p}{T} - 124.9 \dfrac{pq_{\mathrm{t}}}{T}) \times 10^{-6} \\ n_{\mathrm{w}} = (115.9 \dfrac{pq_{\mathrm{t}}}{T} + 6.035 \times 10^5 \dfrac{pq_{\mathrm{t}}}{T^2}) \times 10^{-6}. \end{cases} \quad (4)$$

p, T, and q_{t} correspond to the instantaneous atmospheric pressure, the absolute temperature, and the specific humidity, respectively. n_{d} indicates the contribution of the dry air while n_{w} denotes that of water vapor. The LES generates instantaneous 3D fields of these state variables required to precisely retrieve turbulence parameters. In this letter, a well-documented case of tropical MABL for which a convective cloud layer is located between 500 and 1500 m in altitude is studied [16, 17]. This atmospheric simulation is performed using the open-source code MicroHH [18]. The time evolution of the generated $5 \times 5 \times 3$–km domain is studied for 6 hours with a $50 \times 50 \times 10$–m grid resolution. Note that the first 3 hr of simulation are used to converge toward a statistically steady solution.

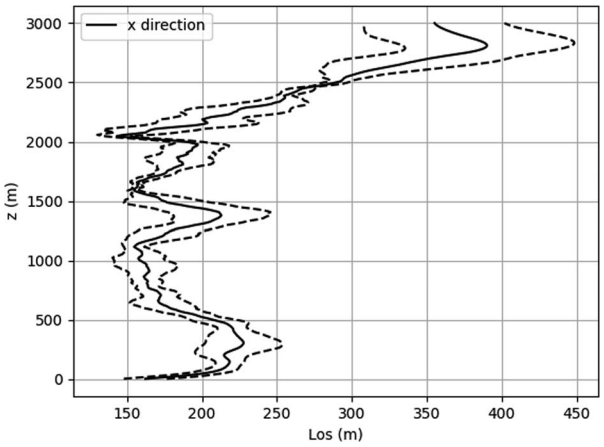

Figure 1. Vertical profile of $L_{\mathrm{os}|x}$ averaged over the last 3 hr (plain line). Dashed lines indicate the ± standard deviation interval.

The objective was to evaluate L_{os} and the vertical profile of $C_n^2(z)$ from the output of the atmospheric LES to insert them into (2) and thus derive a "LES-Kolmogorov" spectrum. To the authors' knowledge, this is the first study to employ LES to introduce a realistic vertical inhomogeneity to turbulent phase screens entirely generated with sMPS.

The outer scale length L_{os} is defined as the largest eddy size within the inertial range of scales of the turbulent flow. A direct computation from LES outputs is not straightforward. However, its value in a given direction $l \in (x, y, z)$ is usually linked to the corresponding integral length scale L_l such that $L_{\mathrm{os}|l} \approx 1/6 L_l$ [19]. Turbulence is here supposed isotropic giving $L_{\mathrm{os}|l} = L_{\mathrm{os}}, \forall\, l \in (x, y, z)$. In particular, the outer scale in the x direction is defined as

$$L_{\mathrm{os}|x} = \frac{1}{6} \int_0^\infty D_{q_{\mathrm{t}}}(r_x) \mathrm{d}r_x, \quad (5)$$

where $D_{q_{\mathrm{t}}}$ indicates the autocorrelation function of the specific humidity. The resulting vertical profile of $L_{\mathrm{os}\,|\,x}$ averaged over the last 3 hr of simulation is plotted in Figure 1. The nonlinear dependency of (2) on the outer scale length makes it difficult to introduce a vertical inhomogeneity of this parameter. In the following, L_{os} is therefore taken equal to its vertical mean value so that

$$L_{\mathrm{os}} = \langle L_{\mathrm{os}|x} \rangle_{t,z} \approx 219\,\mathrm{m}.$$

The turbulent structure constant C_n^2 characterizes the amplitude of the variations of the turbulent refractive index. In the inertial range, this is related to the refractive index autocorrelation function by the Obukhov law so that [6]

$$C_n^2 = \frac{D_n(r)}{r^{2/3}}, \ \forall\, r \in [L_{\mathrm{is}}, L_{\mathrm{os}}], \quad (6)$$

where r is the separation distance. In the x direction, $D_n(r_x)$ is derived from the generated thermodynamic fields using

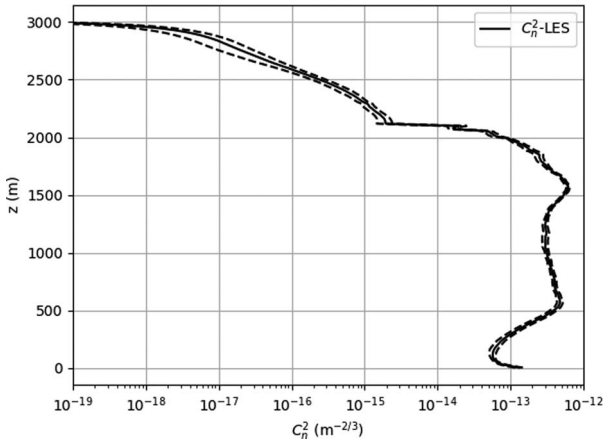

Figure 2. Vertical profile of $C_n^2(z)$ averaged over the last 3 hr (plain line). Dashed lines indicate the ± standard deviation interval.

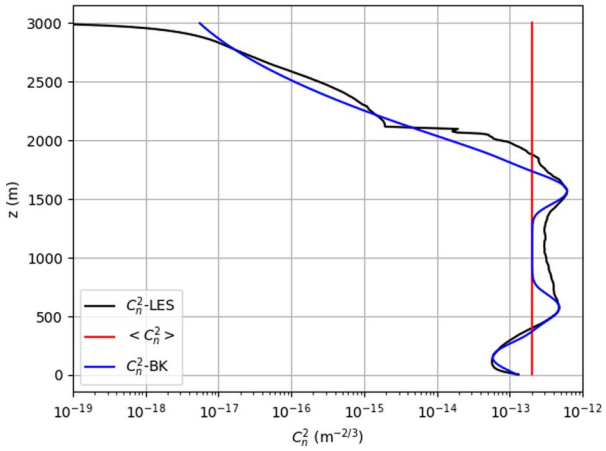

Figure 3. Vertical profiles of $C_n^2(z)$ from LES (black line) and the parametric BK-model (blue line). Red line indicates the equivalent mean profile.

(3) and (4) and is numerically computed following [9]. The condition $r_x < L_{os}(z)$ is applied to satisfy the inertial regime assumption. The value of $C_n^2(z)$ is then obtained by averaging over the different r_x. This algorithm is repeated at each altitude to derive the complete profile. The vertical structure of $C_n^2(z)$ averaged over the last 3 hr of simulation corresponding to the generated MABL is plotted in Figure 2. As expected, it exhibits global inhomogeneities. Indeed, strong turbulence is located within the cloud layer between 500 and 1500 m in altitude while its intensity falls down in the free atmosphere above 2000 m.

2.3 Parametric Model

LES allows for a precise description of atmospheric turbulence and leads to a better understanding of this phenomenon. However, this is very computationally time-consuming. Therefore, it is essential to determine whether a parametric generation of the inhomogeneous turbulence in a MABL can acceptably model the actual effects of the phenomenon on an EM wave.

In the following, we propose to replicate the vertical profile of the turbulent structure constant corresponding to the generated tropical MABL using a parametric Bump-Kolmogorov model (BK model). It consists in locally amplifying or attenuating a reference value that is here set to $\langle C_n^2 \rangle_z$, around a given altitude. This analytical formulation is written as

$$C_n^2(z) = \langle C_n^2 \rangle_z \frac{F(K_2, m_{3,2}, m_{4,2}) F(K_3, m_{3,3}, m_{4,3})}{F(K_1, m_{3,1}, m_{4,1}) F(K_4, m_{3,4}, m_{4,4})}, \quad (7)$$

with

$$F(K_i, m_{3,i}, m_{4,i}) = 1 + K_i \exp\left(\frac{-\left(z - \left(m_{3,i} + \frac{m_{4,i}}{2}\right)\right)^2}{\left(\frac{m_{4,i}}{2}\right)^2} \right). \quad (8)$$

$m_{3,i}$ represents the base height of the i-th bump ($i \in [1, 4]$), $m_{4,i}$ denotes its thickness, and K_i is a modulation coefficient that can be tuned to obtain the desired local maximum or minimum value for $C_n^2(z)$. Note that this parametric model is a generalization of the simple model proposed by Wagner et al. [8]. Their study suggests an arbitrary amplification of a reference C_n^2 value as a single bump within a surface-based duct. In our case, the proposed parametric model enables the replication of a realistic turbulent intensity profile extracted from the LES of a MABL.

The resulting analytical vertical profile of $C_n^2(z)$ is plotted in Figure 3 (blue line) along with the real profile computed from the atmospheric LES (black line) and the corresponding mean value $\langle C_n^2 \rangle_z = 0.204 \times 10^{-12}$ m$^{-2/3}$ (red line). Figure 3 shows that the proposed parametric model is not fully optimal but reasonably approximates a real case. The question is whether the errors made by this model remain acceptable in the case of X-band propagation.

3. Numerical Simulations

This section compares the proposed methods for generating inhomogeneous turbulence via their impact on a radio wave crossing the medium. The objective is 2-fold. First, comparing to an equivalent homogeneous case allows for assessing the specific influence of vertical turbulence inhomogeneity on EM wave propagation. Second, comparing the results obtained from the two methods proposed in Section 2 enables to quantify the error introduced by the parametric BK model.

The propagation of a 10-GHz spherical wave is computed in a free-space environment within a 95 × 3-km domain using the split-step wavelet method [2]. In this theoretical study, the source is located at x = 0 m and z = 1500 m. The turbulent phase screens are generated with the sMPS method using the two proposed models, referred to as the LES-Kolmogorov and BK model, or a homogeneous Von-Karman Kolmogorov spectrum. The propagation step Δ_x, which also indicates the distance separating each turbulent phase screen, is

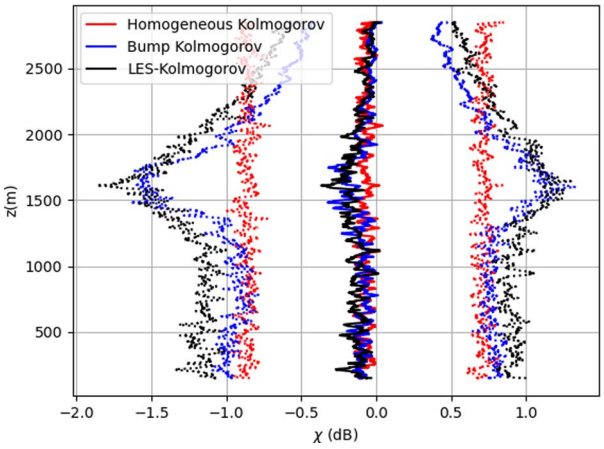

Figure 4. Vertical log-amplitude profiles at $x = 95$ km averaged over 500 simulations and obtained using LES-Kolmogorov (black line), BK model (blue line) and Homogeneous Kolmogorov (red line) spectra. Dotted lines indicate the ± standard deviation interval.

set to 1000 m to satisfy the Markov approximation ($\Delta_x \gg L_{os}$) and thus prevent, correlation effects.

Propagation results are analyzed through the computation of the final vertical log-amplitude profile $\chi(z)$ defined as

$$\chi(z) = \ln\left(\frac{|E_t(z)|}{|E_0(z)|}\right), \tag{9}$$

where E_t and E_0 indicate the real propagated electric field and the one that would have been propagated in a turbulent-free atmosphere, respectively. This metric locally quantifies the impact of turbulence on the propagating field. Results are averaged over 500 simulations. Mean log-amplitude vertical profiles at x = 95 km obtained for each of the three methods are plotted in Figure 4. The dotted lines indicate the ± standard deviation interval. This first illustrates the impact of turbulence inhomogeneity. Although the average turbulence intensity encountered is equivalent, an inhomogeneous vertical distribution of $C_n^2(z)$ leads to a different outcome compared with the homogeneous case. Indeed, the turbulence inhomogeneity of the case studied in this article results in an attenuation peak of around 1600 m, both using the LES-Kolmogorov and BK models. This altitude coincides with the local maximum of $C_n^2(z)$ plotted in Figure 3. However, this local attenuation phenomenon is absent around 650 m, that is, the altitude of the second turbulence peak. This difference occurs because, in the case of spherical waves, the source altitude also has an influence on the EM propagation through inhomogeneous turbulence. Moreover, Figure 4 shows very good agreements between the realistic LES-Kolmogorov approach and the parametric BK model. Specifically, the two methods both exhibit a peak of attenuation around the source altitude. Furthermore, in both cases, the attenuation due to turbulence decreases to the point where it becomes weaker than that induced by a homogeneous modeling above 2250 m. The observed behavior aligns with the decrease in the turbulence intensity illustrated in Figure 3. These initial results suggest both the importance of considering turbulence inhomogeneity in the MABL and the feasibility of an accurate parametric modeling approach.

4. Conclusion

This letter introduces two original methods for generating realistic inhomogeneous turbulence with the classical sMPS approach have been introduced. The LES-Kolmogorov method is based on the extraction of an accurate vertical profile of $C_n^2(z)$ from thermodynamic parameters generated by atmospheric simulations. In contrast, the BK model approximately reproduces the obtained profile with a parametric model.

The free-space propagation of a 10-GHz spherical wave over 95 km has been analyzed through the computation of log-amplitude profiles. The specific local impact of turbulence inhomogeneity has first been highlighted through the comparison with an equivalent homogeneous case. Furthermore, the two proposed methods yield similar results, suggesting that a parametric replication of turbulence inhomogeneity in the ABL is a reasonable approach.

In future works, equivalent studies at higher frequencies and on other cases of atmospheric simulations would be interesting to draw definitive conclusions about the accuracy of the proposed parametric model in reproducing turbulence within a MABL. Moreover, additional research is required to highlight the impact of the source position on the propagation of a spherical wave within inhomogeneous turbulence. Ultimately, a sensitivity analysis would allow us to propose a simpler yet accurate parametric profile for turbulence.

5. References

1. D. Dockery and J.R. Kuttler, “An Improved Impedance-Boundary Algorithm for Fourier Split-Step Solutions of the Parabolic Wave Equation,” *IEEE Transactions on Antennas and Propagation*,” **44**, 12, December 1996, pp. 1592–1599.
2. H. Zhou, R. Douvenot, and A. Chabory, “Modeling the Long-Range Wave Propagation by a Split-Step Wavelet Method,” *Journal of Computational Physics*, **402**, February 2020, p. 109042.
3. V. Fabbro and L. Feral, “Comparison of 2D and 3D Electromagnetic Approaches to Predict Tropospheric Turbulence Effects in Clear Sky Conditions,” *IEEE Transactions on Antennas and Propagation*, **60**, 9, July 2012, pp. 4398–4407.
4. V. Darchy, R. Douvenot, H. Galiègue, and S. Jamme, “Discrete Turbulent Spectrum Modelling for 2D Split--Step Electromagnetic Propagation Schemes,” 2023 17th European Conference on Antennas and Propagation (EuCAP), Florence, Italy, March 26–31, 2023, pp. 1–5.
5. S. Mukherjee and C. Yardim, “Accurate computation of Scintillation in Tropospheric Turbulence with Parabolic Wave Equation,” *IEEE Transactions on Antennas and Propagation*, **69**, 8, February 2021, pp. 4748–4757.

6. V. I. Tatarskii. *The Effects of the Turbulent Atmosphere on Wave Propagation*. Jerusalen, Israel, Israel Programm for Scientific Translations, 1971.
7. M. Chamecki and N. L. Dias, "The Local Isotropy Hypothesis and the Turbulent Kinetic Energy Dissipation Rate in the Atmospheric Surface Layer," *Quarterly Journal of the Royal Meteorological Society*, **130**, 603, October 2004, pp. 2733–2752.
8. M. Wagner, P. Gerstoft, and T. Rogers, "Estimating Refractivity from Propagation Loss in Turbulent Media," *Radio Science*, **51**, 12, November 2016, pp. 1876–1894.
9. C. Wilson and E. Fedorovich, "Direct Evaluation of Refractive-Index Structure Functions from Large-Eddy Simulation Output for Atmospheric Convective Boundary Layers," *Acta Geophysica*, **60**, September 2012, pp. 1474–1492.
10. R. Stoll, J. A. Gibbs, S. T. Salesky, W. Anderson, and M. Calaf, "Large-Eddy Simulation of the Atmospheric Boundary Layer," *Boundary-Layer Meteorology*, **177**, August 2020, pp. 541–581.
11. K. E. Gilbert, X. Di, S. Khanna, M. J. Otte, and J. C. Wyngaard, "Electromagnetic Wave Propagation Through Simulated Atmospheric Refractivity Fields," *Radio Science*, **34**, 6, November 1999, pp. 1413–1435.
12. V. Darchy, R. Douvenot, S. Jamme, and H. Galiègue, "Investigation on Vertical Resolution of Atmospheric Simulations for the Propagation in Realistic Turbulent Media," 2023 IEEE-APS Topical Conference on Antennas and Propagation in Wireless Communications (APWC), Venice, Italy, October 9–13, 2023, pp. 86–89.
13. S. Avramov-Zamurovic, K. P. Judd, S. Matt, R. A. Handler, A. T. Watnik, et al., "Propagating Beams Carrying Orbital Angular Momentum Through Simulated Optical Turbulence Generated by Rayleigh–Bénard Natural Convection," *Waves in Random and Complex Media*, **0**, 0, June 2023, pp. 1–21.
14. T. Von Karman, "Progress in the Statistical Theory of Turbulence," *Proceedings of the National Academy of Sciences*, **34**, 11, November 1948, pp. 530–539.
15. A. Tunick, "Cn2 Model to Calculate the Micrometeorological Influences on the Refractive Index Structure Parameter," *Environmental Modelling and Software*, **18**, 2, March 2003, pp. 165–171.
16. A. P. Siebesma, C. S. Bretherton, A. Brown, A. Chlond, J. Cuxart, et al., "A Large Eddy Simulation Intercomparison Study of Shallow Cumulus Convection," *Journal of the Atmospheric Sciences*, **60**, 10, May 2003, pp. 1201–1219.
17. A. Dipankar and P. Sagaut, "A New Phase-Screen Method for Electromagnetic Wave Propagation in Turbulent Flows Using Large-Eddy Simulation," *Journal of Computational Physics*, **228**, November 2009, pp. 7729–7741.
18. C. C. van Heerwaarden, B. J. H. van Stratum, T. Heus, J. A. Gibbs, E. Fedorovich, et al., "Microhh 1.0: A Computational Fluid Dynamics Code for Direct Numerical Simulation and Large-Eddy Simulation of Atmospheric Boundary Layer Flows," *Geoscientific Model Development*, **10**, 8, August 2017, pp. 3145–3165.
19. S.B. Pope and P.J. Eccles, *Turbulent Flows*. Cambridge, UK, Cambridge University Press, 2000.